Determining Land Subsidence in Western Taiwan by Using a New Approach of Weighting PS-InSAR with Redundant Observations

Jun-Fu Ye[1] and Jaan-Rong Tsay[2]
[1] National Cheng Kung University, No. 1, University Road, Tainan City 701, Taiwan,
Email: junfu.ye@gmail.com
[2] National Cheng Kung University, No. 1, University Road, Tainan City 701, Taiwan,
Email: tsayjr@mail.ncku.edu.tw

KEY WORDS: PS-InSAR, Redundant Observations, Weight, Accuracy, Reliability

ABSTRACT: Since the emerging of the technique of persistent scatterer interferometric synthetic aperture radar (PS-InSAR), diverse algorithms and methods are developed for finding stable scatterers. Also, different models and approaches are proposed for reducing phase errors caused by diverse influencing factors such as atmospheric sphere, topographic characteristics and noise. Then, the terrain surface deformation velocity at each persistent scatterer (PS) is determined. Although PS-InSAR is already widely applied for monitoring low-speed terrain surface deformation velocity component, most researches study mainly on the estimation of linear deformation velocity. Therefore, this paper presents a new approach for improving the data processing of PS-InSAR. Moreover, some ground check data are used to evaluate the quality of PS-InSAR on monitoring terrain surface deformation. In order to increase the robustness of PS-InSAR, the technique of redundant observation in the field of surveying and geomatics is utilized on the one hand. For each computation of PS-InSAR, different sets of SAR images in the same time period are adopted so that the ability of blunder detection is increased. On the other hand, the decorrelation effect caused by diverse factors is taken into account so that different weights are given to all sets of SAR images. Weighting averages are then computed to determine the most probable deformation velocity vectors on all scatterers. Higher outer reliability is expected. Finally, the results are compared with the ground check data determined by high precision levelling. Their quality is thus estimated.

1. INTRODUCTION

Taiwan has many natural disasters, such as typhoons and earthquakes, because it is located in a special geographical area. In addition, human activities also lead to the topographical changes, such as landslide and land subsidence. Therefore, it is essential for long-term monitoring topographical deformation and short-term land cover change detection in Taiwan. Synthetic aperture radar (SAR) is an active microwave imaging radar. It not only has the advantage of overcoming the limitations of daylight and weather conditions but also can obtain rapidly a wide range of terrain surface information simultaneously.

Diverse SAR techniques are used to monitor terrain deformation, such as differential interferometric synthetic aperture radar (D-InSAR), PS-InSAR, and temporarily coherent point InSAR (TCP-InSAR). A lot of research has shown that D-InSAR can determine effectively the terrain displacement in an area with higher coherence (Massonnet et al., 1995; Amelung et al., 2000). However, a longer temporal baseline is required to detect low-velocity terrain displacement, and it decreases the quality of the result by D-InSAR method due to lower coherence caused by temporal decorrelation. PSs and TCPs are extracted by searching persistently higher coherent points in the different SAR image pairs. Therefore, PS-InSAR and TCP-InSAR can be used to monitor low-velocity terrain deformation.

Ferretti et al. (2000; 2001) originally proposed a complete PS-InSAR procedure to determine the displacement velocities on PSs. The PS candidates (PSCs) can be extracted from several SAR images based on pixel strength. The pixel, whose strength is larger than or equal to a specific strength threshold, is selected as a PSC. The number of adopted SAR images must be larger than thirty for this method to perform a correct statistical study. Finally, each PS, which is extracted from the PSCs, can estimate the displacement velocity by using PS-InSAR. Mora et al. (2003) proposed a simple and effective PSInSAR method. The PSCs are extracted from the coherence images based on coherence threshold. In addition, the number of adopted SAR images only needs to larger than seven. In this study, the related PS-InSAR processing is referred to (Mora et al., 2003). In order to obtain reliable PS-InSAR results, this paper used the concept of redundant observations and weighted average to evaluate the quality of PS-InSAR results.

2. METHODOLOGY

2.1 PS-InSAR

In physics, the term coherence can be defined as the correlation between waves observed at different moments or different points. When the waves are observed at different moments in time have high consistency, it means that it has good temporal coherence. And when the waves are observed at different points in space have high consistency, it means that it has good spatial coherence. In synthetic aperture radar, the coherence can describe the correlation between SAR images from different sampling time or space, and it can be defined as the complex cross-correlation coefficient of the SAR images. Based on Rosen et al. (2000), the coherence value can be defined as

$$\gamma = \frac{|\sum g_1 \cdot g_2^*|}{\sqrt{\sum |g_1|^2 \cdot \sum |g_2|^2}} = |\gamma| \cdot e^{j\Phi_0} \tag{1}$$

where g_i denotes the SAR return at the *i* antenna, and g_2^* is the complex conjugate of g_2. For $\gamma = 1$, it indicates that the two conjugate pixels are completely correlation; for $\gamma = 0$, it indicates that the two conjugate pixels are no correlation. The PSCs are selected when its coherence in all of the adopted coherence images is larger than the coherent threshold value. In interferograms, the phase variation between two neighboring PSCs, which are connected by Delaunay triangulation, can be expressed as (Mora et al., 2003)

$$\delta\phi_{int} = \delta\phi_{flat} + \delta\phi_{topo} + \delta\phi_{mov} + \delta\phi_{atm} + \delta\phi_{noise} \tag{2}$$

where $\delta\phi_{flat}$ is the phase variation component related with range distance in flat earth; $\delta\phi_{topo}$ is topographic phase; $\delta\phi_{mov}$ is the phase variation component derived from terrain displacement along slant-range direction between two SAR acquisitions; $\delta\phi_{atm}$ is the phase variation component of atmospheric artifacts; $\delta\phi_{noise}$ includes the others phase decorrelation factors, such as temporal decorrelation, spatial decorrelation and thermal noise. However, $\delta\phi_{flat}$ and $\delta\phi_{topo}$ can be removed through D-InSAR processing. In differential interferograms, the phase variation between two neighboring PSCs can be expressed as (Mora et al., 2003)

$$\delta\phi_{dif} = \delta\phi_{topoerror} + \delta\phi_{mov} + \delta\phi_{atm} + \delta\phi_{noise} \tag{3}$$

where $\delta\phi_{topoerror}$ is the phase variation component caused by eliminating topographic effect incompletely, and it can be expressed as (Mora et al., 2003)

$$\delta\phi_{topoerror} = \frac{4 \cdot \pi}{\lambda \cdot r} \cdot \frac{B \cdot \Delta\varepsilon}{\sin\theta} \tag{4}$$

where λ is the wavelength of radar wave; r is the slant-range between radar antenna and ground target; B is the spatial baseline; $\Delta\varepsilon$ is the increment of height error; θ is the incidence angle. $\delta\phi_{mov}$ includes linear and nonlinear component, and it can be expressed as (Mora et al., 2003)

$$\delta\phi_{mov} = \delta\phi_{lin} + \delta\phi_{nonlin} = \frac{4 \cdot \pi}{\lambda} \cdot T \cdot \Delta v + \Delta\beta \tag{5}$$

where T is the temporal baseline; Δv is the increment of linear displacement velocity component between two neighboring PSCs; $\Delta\beta$ is the nonlinear displacement velocity component. Based on the aforementioned equations, (3) can be expressed as (Mora et al., 2003)

$$\begin{aligned}\delta\phi_{dif}(x_m, y_m, x_n, y_n, T_i) = {} & \frac{4 \cdot \pi}{\lambda \cdot r(T_i)} \cdot \frac{B(T_i)}{\sin(\theta_i)} \cdot [\varepsilon(x_m, y_m) - \varepsilon(x_n, y_n)] + \frac{4 \cdot \pi}{\lambda} \cdot T_i \cdot [v(x_m, y_m) - v(x_n, y_n)] \\ & + [\beta(x_m, y_m, T_i) - \beta(x_n, y_n, T_i)] + [\alpha(x_m, y_m, T_i) - \alpha(x_n, y_n, T_i)] + [n(x_m, y_m, T_i) - n(x_n, y_n, T_i)]\end{aligned} \tag{6}$$

where (x_m, y_m) and (x_n, y_n) are the image coordinates of two neighboring PSCs in a local 2D Cartesian coordinate system; T_i is the temporal baseline of the *i*th interferogram; α is the atmospheric phase artifacts; n is the phase decorrelation noise. The atmospheric phase artifacts can be regarded as a random value because atmospheric conditions are variable. However, the atmospheric conditions can be considered as the similar for two connected PSCs when the horizontal distance is less than 1 kilometer (Hanssen, 1998). In this way, atmospheric artefacts can be assumed as (Mora et al., 2003)

$$\alpha(x_m, y_m, T_i) \approx \alpha(x_n, y_n, T_i) \tag{7}$$

Because $\delta\phi_{topoerror}$ and $\delta\phi_{lin}$ are regarded as constants in all of the differential interferograms, they can be estimated by modelling as follows: (Ferretti et al., 2001)

$$\delta\phi_{model}(x_m, y_m, x_n, y_n, T_i) = \frac{4\cdot\pi}{\lambda\cdot r(T_i)}\cdot\frac{B(T_i)}{\sin(\theta_i)}\cdot[\varepsilon_{model}(x_m, y_m) - \varepsilon_{model}(x_n, y_n)] + \frac{4\cdot\pi}{\lambda}\cdot T_i\cdot[v_{model}(x_m, y_m) - v_{model}(x_n, y_n)] \quad (8)$$

It can be calculated by maximizing the model coherence function as follows: (Ferretti et al., 2001)

$$\gamma_{model}(x_m, y_m, x_n, y_n, T_i) = \frac{1}{N}\cdot\left|\sum_{i=0}^{N}\exp\left[j\cdot\left(\delta\phi_{dif}(x_m, y_m, x_n, y_n, T_i) - \delta\phi_{model}(x_m, y_m, x_n, y_n, T_i)\right)\right]\right| \quad (9)$$

where N is the number of the adopted differential interferograms. When this function (9) is closer to one, the total decorrelation is closer to zero. The PSCs are selected as PSs when $\gamma_{model}(x_m, y_m, x_n, y_n, T_i)$ is large than the threshold of model coherence function; on the contrary, the PSCs are rejected. Then, the increment of linear displacement velocity component and topographic error can be expressed as

$$\Delta v_{estimated}(x_m, y_m, x_n, y_n) = [v_{model}(x_m, y_m) - v_{model}(x_n, y_n)]_{maximize\ \gamma} \quad (10)$$

$$\Delta\varepsilon_{estimated}(x_m, y_m, x_n, y_n) = [\varepsilon_{model}(x_m, y_m) - \varepsilon_{model}(x_n, y_n)]_{maximize\ \gamma} \quad (11)$$

According to Xu and Cumming (1999), the linear displacement velocity can be estimated by using the classical region growing algorithm for phase unwrapping.

2.2 Redundant Observations and Weighted Average

In surveying engineering, true value cannot be obtained because surveying results are affected by many factors, such as instrument structure, human error, and natural environment. Therefore, quality assessment becomes an important role in practical applications. In general, redundancy is a common method to reduce the possibility of error. And the precision, accuracy and reliability of surveying results, which are determined from redundant observations, are the fundamental figures. We use the concept of redundant observations in surveying engineering for acquiring a reliable result determined by PS-InSAR. This method applies the same group of SAR images which are acquired in the same time duration to provide several combinations of image pairs, and then we use these combinations of image pairs to generate several sets of PS-InSAR results with redundancy. Checking the variation of these results can determine the precision and the reliability of PS-InSAR results.

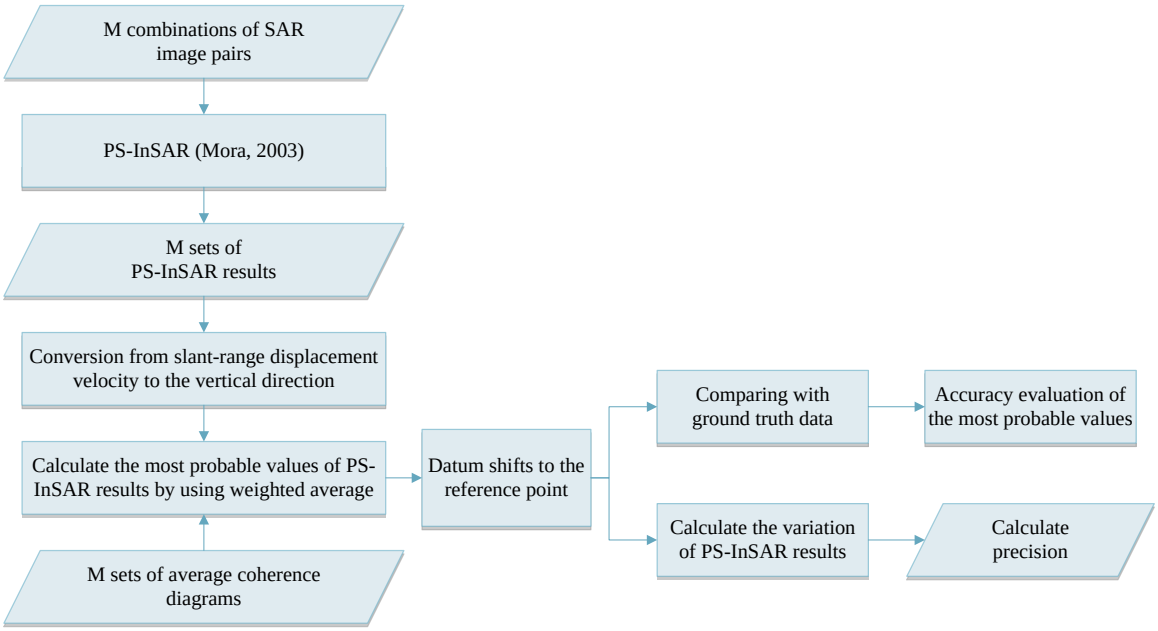

Figure 1. The flowchart of a weighting PS-InSAR with redundant observations

In synthetic aperture radar, coherence can be defined as the complex cross-correlation coefficient of the SAR images. However, the coherence may be affected by several factors, such as spatial decorrelation (γ_{geom}), temporal decorrelation ($\gamma_{temporal}$), Doppler Centroid decorrelation (γ_{DC}), volume decorrelation (γ_{vol}), thermal noise decorrelation ($\gamma_{thermal}$), and imperfect image processing ($\gamma_{processing}$) (Zebker and Villasenor, 1992；Soergel, 2013). The entire coherence (γ) of interferograms can be denoted as the product of those factors (Soergel, 2013).

$$\gamma = \gamma_{geom} \cdot \gamma_{temporal} \cdot \gamma_{DC} \cdot \gamma_{vol} \cdot \gamma_{thermal} \cdot \gamma_{processing} \tag{12}$$

The purpose of weighted average is that higher quality observations have higher proportion. When the influence of random errors can be as low as possible, we can obtain more reliable results for the most probable values. Based on this premise, on the on hand blunders and system errors must be removed from observations, and on the other hand we need to consider how to define the weights in this study. The former can be compared with ground truth data or evaluated from the redundant observations. We consider through the characteristic of coherence to determine the latter because high coherence denotes high consistency. In this study, we attempts to use the square of average coherence of each set of SAR images as weighting.

3. EXPERIMENT AND ANALYSIS

According to the information from land-subsidence prevention and reclamation Corp. (LSPRC), National Cheng Kung University (NCKU) and Water Resources Agency (WRA), Ministry of Economic Affairs, Taiwan, some areas in Taiwan have long-term land subsidence, especially in Changhua and Yunlin County of western Taiwan. The interest area in this study is about 10 km × 10 km in Sihu, Changhua, Taiwan. We adopted 12 SAR images in this study, and the specification of experimental images are shown as Table 1.

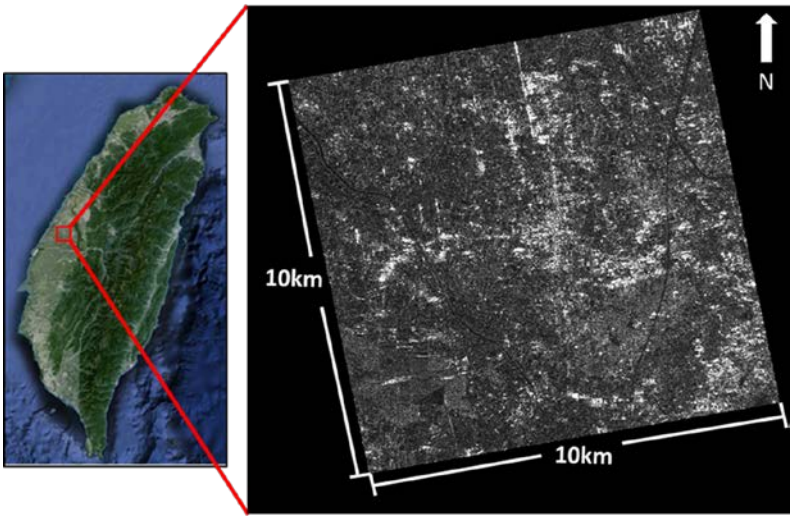

Figure 2. The interest area in this study

Table 1. The specification of experimental images

Satellite	ALOS
Sensor	PALSAR
Center Frequency	1270 MHz (L-band)
Orbit Number	446
Frame Number	460
Acquisition Time	2007/08/18 ~ 2010/11/26
Acquisition Mode	FBD
Polarization	HH
Orbit Direction	Ascending
Ground Coverage	10 km × 10 km
Incidence Angle	38.1 deg.
Orbit Altitude	691.65 km

Table 2. Multi-combination of SAR image pairs (●: master image; ○: slave image)

ID.	1	2	3	4	5	6	7	8	9	10	11	12
I	○	●	○	○		○	○	○	○	○	○	○
II	○	○	●				○	○	○	○	○	○
III	○	○		●	○	○	○	○	○	○	○	○
IV	○	○	○	○	○	○	●		○	○	○	○
V	○	○	○	○	○	○		●	○	○	○	○
VI	○	○	○	○			○	○	●	○	○	○
VII	○	○	○	○			○	○	○	●	○	○
VIII	○	○	○	○			○	○	○	○	●	○

Table 2 shows each combination of SAR images, and a few images are not used in some combination due to low coherence. Three conditions are used to filter the coherence images, including (1) maximum coherence must be greater than 0.7 (2) normal baseline must be less than 1800 m (3) coherence is greater than 0.25 at least ten percent. Image 7 and 8 are used to calculate topographic pair because they have the shortest temporal baseline and second short normal baseline, and they can provide better topographic phase in theory.

In this study, we used levelling data as the ground truth data, which be measured annually by Water Resources Agency, Ministry of Economic Affairs, Taiwan, and its acquisition time is from July 2007 to June 2010. Datum transformation is essential to compare the results of PS-InSAR and levelling. Therefore, we selected one levelling point as a datum point.

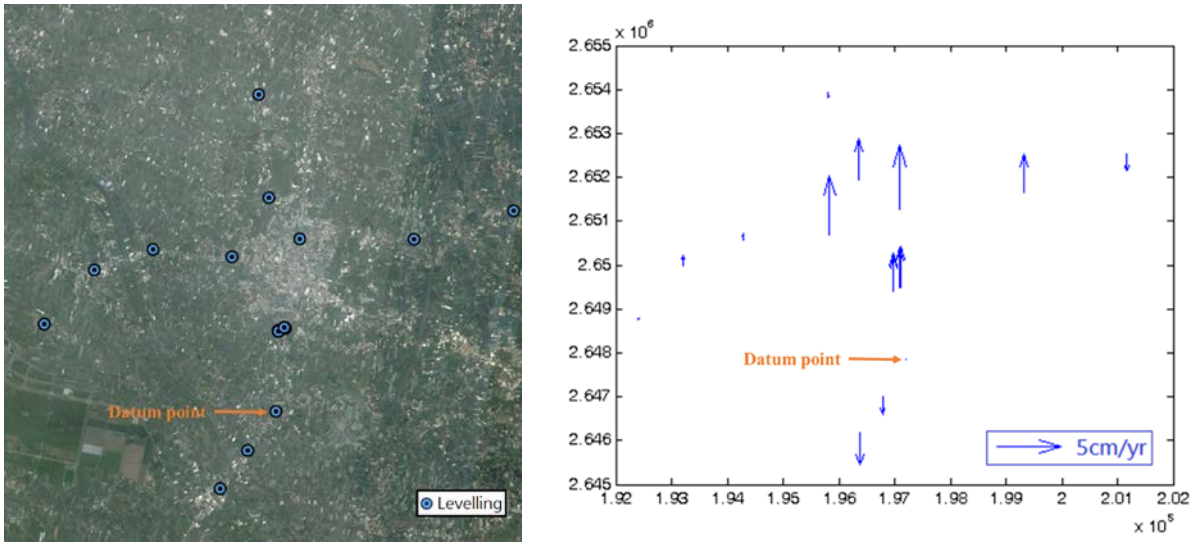

Figure 3. (Left) The distribution of ground truth data and datum point, and (right) their error vectors of PS-InSAR results.

Figure 3 shows the distribution of ground truth data and datum point, but we can find the difference between urban area and non-urban area through their error vectors. According to the information from LSPRC, wet season in Changhua County is from May to September. In order to confirm the association with the wet and dry seasons, we try to make the image acquisition time as close as possible to the ground truth data. However, this case still has similar results. Thus, we considered that SAR may have different scattering characteristics under different environments. To verify this possibility, we used a statistical test to decide whether both of them are the same population. The population is so small that we do not have enough confidence to confirm that it complies the assumption of normal distribution, so we use the Mann–Whitney U test which is one of the nonparametric statistical methods. The statistical test result shows that the null hypothesis is rejected under the 95% confidence level, so they belong to different population. As shown in Figure 4, we selected second levelling point as a datum point in urban area. The average difference in whole area is less than 1.0 cm/yr, and the RMSD is about 1.0 cm/yr. The magnitude of improvement is about 14.0% to 50.4%. It shows weighting PS-InSAR method with redundant observations can obtain more accurate results.

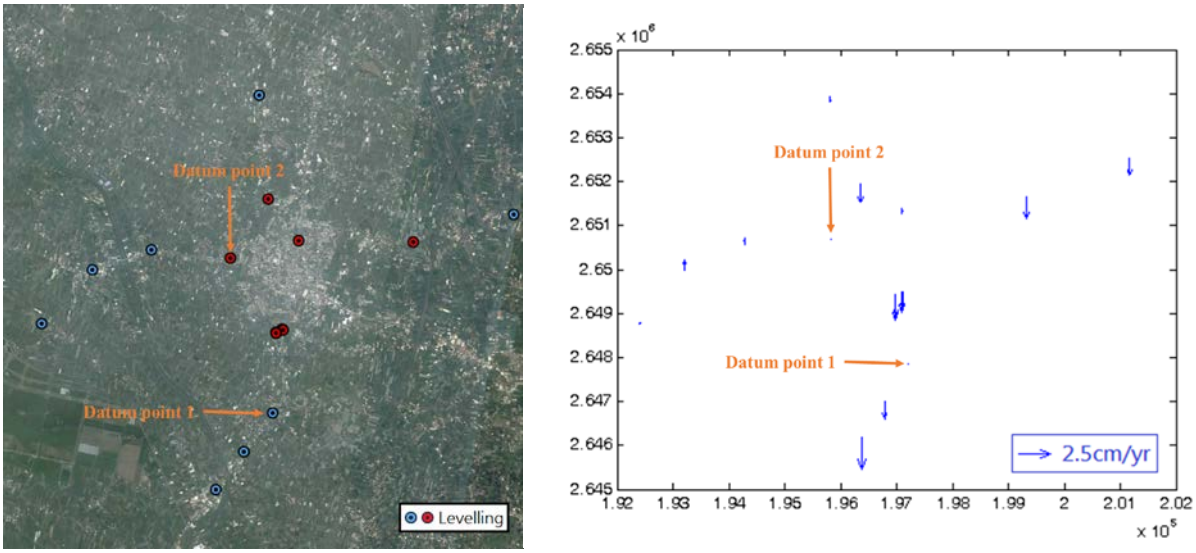

Figure 4. (Left) The distribution of ground truth data and datum point, and (right) their error vectors of PS-InSAR results.

Table 3. The statistics for the difference between PSs and levelling

	All region	Urban Area	Non-urban Area
Average (cm/yr)	-0.8	-0.5	-1.2
RMSD (cm/yr)	1.0	1.0	0.8

Table 4. The accuracy and percentage improvement in each combination

i	σ_i (cm/yr)	$P = \frac{\sigma_i - \sigma_{avg}}{\sigma_i} \times 100\%$
I	1.71	42.0%
II	1.70	41.5%
III	1.49	33.4%
IV	1.29	23.1%
V	1.15	14.0%
VI	1.74	42.9%
VII	2.00	50.4%
VIII	1.21	18.3%
Weighted average	0.99	-

4. CONCLUSIONS

In order to increase the robustness of PS-InSAR, this paper proposes a new approach of weighting PS-InSAR with redundant observations. The conclusions are summarized as follows: (1) The difference between the average vertical displacement velocities of PSs and levelling is less than 1.0 cm/yr. It shows PS-InSAR method can be used to detect land subsidence. (2) Through the way of the redundant observations and weighted average, the results of PS-InSAR can obtain better accuracy and more robustness. (3) The scatterers may have different scattering characteristics under different environment types, so classification can effectively reduce their influence.

REFERENCES

Amelung, F., Jonsson, S., Zebker, H., and Segall, P., 2000. Widespread Uplift and Trap Door Faulting on Galapagos Volcanoes Observed with Radar Interferometry, Nature, Vol. 407, pp. 993-996.

Ferretti, A., Prati, C., and Rocca, F., 2000. Nonlinear Subsidence Rate Estimation Using Permanent Scatterers in Differential SAR Interferometry, IEEE Transactions on Geoscience and Remote Sensing, Vol. 38, No. 5, pp. 2202-2212.

Ferretti, A., Prati, C., and Rocca, F., 2001. Permanent Scatterers in SAR Interferometry, IEEE Transactions on Geoscience and Remote Sensing, Vol. 39, No. 1, pp. 8-20.

Hanssen, R., 1998. Atmospheric Heterogeneities in ERS Tandem SAR Interferometry, DEOS Report No.98.1, Delft

University press, Delft, Netherlands.
Massonnet, D., Briole, P., and Arnaud, A., 1995. Deflation of Mount Etna Monitored by Spaceborne Radar Interferometry, Nature, Vol. 375, No. 15, pp. 567-570.
Mora, O., Mallorqui, J. J., and Broquetas, A., 2003. Linear and Nonlinear Terrain Deformation Maps from a Reduced Set of Interferometric SAR Images, IEEE Transactions on Geoscience and Remote Sensing, Vol. 41, No. 10, pp. 2243-2253.
Rosen, P.A., Hensley, S., Joughin, I.R., Li, F.K., Madsen, S.N., Rodríguez, E. and Goldstein R.M., 2000. Synthetic Aperture Radar Interferometry – Invited Paper, Proceedings of IEEE, Vol. 88, No. 3, pp. 333-382.
Soergel, U., Jacobsen, K., and Schack, L., 2013. The TanDEM-X Mission: Data Collection and Deliverables, Photogrammetric Week 2013.
Xu, W. and Cumming, I., 1999. A region-growing algorithm for InSAR phase unwrapping, IEEE Transactions on Geoscience and Remote Sensing, Vol. 37, No. 1, pp. 124-134.
Zebker, H. A. and Villasenor, J., 1992. Decorrelation in interferometric radar echoes, IEEE Transactions on Geoscience and Remote Sensing, Vol. 30, No. 5, pp. 950-959.